

Galactic masers: kinematics, spiral structure and the disk dynamic state

A. S. Rastorguev^{1,2,3} \star , N. D. Utkin^{1,2,3}, M. V. Zabolotskikh^{1,2}, A. K. Dambis^{1,2},
A. T. Bajkova⁴ and V. V. Bobylev⁴

¹Lomonosov Moscow State University, 1, Leninskie Gory, Moscow, 119991, Russia

²Sternberg Astronomical Institute, 13, Universitetskii prospect, Moscow, 119992, Russia

³Lomonosov Moscow State University, Faculty of Physics, 1, bld.2, Leninskie Gory, Moscow, 119992, Russia

⁴Central (Pulkovo) Astronomical Observatory, Russian Academy of Sciences, 65/1 Pulkovskoye Chaussee, St. Petersburg, 196140, Russia

Received 2016 March, 3; Accepted 2016 November, ??

ABSTRACT

We applied the currently most comprehensive version of the statistical-parallax technique to derive kinematical parameters of the maser sample with 136 sources. Our kinematic model comprises the overall rotation of the Galactic disk and the spiral density-wave effects. We take into account the variation of radial velocity dispersion with Galactocentric distance. The best description of the velocity field is provided by the model with constant radial and vertical velocity dispersions, $(\sigma U_0, \sigma W_0) \approx (9.4 \pm 0.9, 5.9 \pm 0.8)$ km/s. We compute flat Galactic rotation curve over the Galactocentric distance interval from 3 to 15 kpc and find the local circular rotation velocity to be $V_0 \approx (235 - 238)$ km/s ± 7 km/s. We also determine the parameters of the four-armed spiral pattern (pitch angle $i \approx (-10.4 \pm 0.3)^\circ$ and the phase of the Sun $\chi_0 \approx (125 \pm 10)^\circ$). The radial and tangential spiral perturbations are about $f_R \approx (-6.9 \pm 1.4)$ km/s, $f_\Theta \approx (+2.8 \pm 1.0)$ km/s. The kinematic data yield a solar Galactocentric distance of $R_0 \approx (8.24 \pm 0.12)$ kpc. Based on rotation curve parameters and the asymmetric drift we infer the exponential disk scale $H_D \approx (2.7 \pm 0.2)$ kpc under assumption of marginal stability of the intermediate-age disk, and finally we estimate the minimum local surface disk density, $\Sigma(R_0) > (26 \pm 3) M_\odot \text{pc}^{-2}$.

Key words: Methods: data analysis – Galaxy: kinematics and dynamics

1 INTRODUCTION

The kinematics of Galactic disk populations has remained a focus of persistent interest for many decades. The main task was and remains the computation of the rotation curve of the disk, which reflects the features of the mass distribution in the Galaxy and is often used, especially by radio astronomers, to estimate the kinematic distances to objects. To determine the run of the rotation curve the researchers mostly used samples of young Galactic-disk objects with bona fide distances (i.e., with distances determined with relatively small random errors): Cepheids, young open clusters, *HII* clouds, star-forming regions, OB stars, OB associations, red-clump giants, etc. (Burton and Gordon 1978; Fich et al. 1989; Brand and Blitz 1993; Dambis et al. 1995; Glushkova et al. 1998, 1999; Melnik et al. 1999; Rastorguev et al. 1999; Dambis et al. 2001a,b; Melnik et al. 2001a,b; Zabolotskikh et al. 2002; Bobylev 2004;

Bobylev et al. 2006, 2007, 2008; Melnik and Dambis 2009; Bobylev et al. 2009; Bobylev and Bajkova 2013a). Demers and Battinelli (2007) used carbon stars to trace the run of the rotation curve beyond the solar circle out to a Galactocentric distance of 15 kpc and then extended their study to the Galactocentric distance of 24 kpc (Battinelli et al. 2013). Bovy et al. (2012) performed a detailed analysis of the kinematics of an extensive sample of red giants studied within the framework of the SDSS-III/APOGEE project (Eisenstein et al. 2011) in the Galactocentric distance interval $4 < R < 14$ kpc. The authors of a number of recent studies (e.g., Sofue (2012) and Bhattacharjee et al. (2014)) attempt to combine the disk rotation curve constructed for the central region of the Galaxy with the kinematic data for distant stars of the Galactic halo described by stellar hydrodynamics equations.

Khoperskov and Tyurina (2003) and Sofue et al. (2009) demonstrate the large scatter of the circular velocities of different objects inferred by different authors, which casts doubt on the reliability of kinematic distances determined

\star E-mail: rastor@sai.msu.ru

using the rotation curve. This scatter can mostly be explained by the use of inconsistent distance scales for different objects, different adopted values of the solar Galactocentric distance, use of different techniques for analyzing the space velocity field, and the neglect of the effects associated with the deviation of the mass distribution from axial symmetry (i.e., the influence of the bar and spiral density waves).

Of great importance for modelling the Milky Way is the issue of the effect of a massive Galactic bar on the kinematics of the disk, primarily on the run of the rotation curve in the Galactocentric distance interval $R < 4$ kpc. It is now perhaps safe to say that the asymmetry of the *HI* rotation curve first found by Kerr (1964, 1969) using the tangent-point method and confirmed by later studies, e.g., Levine et al. (2008), is due to this very effect. A simulation of the effect of the massive Galactic bar on the results of the determination of the run of the rotation curve in the central part of the Galaxy (Chemin et al. 2015) strongly supports this point of view. In particular, the above authors showed that ignoring these effects when decomposing the rotation curve may result in overestimating the bulge mass by a factor of several times. In this case the computed rotation curve in the central region within about 2 kpc lies systematically above the “true” rotation curve.

The buildup of observational data for maser sources in Galactic star-forming regions (see the review by Reid and Moran (1981)) opened up new prospects for a detailed analysis of the state and kinematics of the thin Galactic disk. The authors of recent studies (Reid et al. 2009; Stepanishchev and Bobylev 2011; Bajkova and Bobylev 2012, 2013; Bobylev and Bajkova 2013c; Reid et al. 2014; Bobylev and Bajkova 2014a,b,c) used maser sources to trace the rotation curve and estimate the parameters of the spiral pattern of our Galaxy. In addition, Bobylev and Bajkova (2013b) estimated the pitch angle of the Milky-Way spiral pattern from the space distribution of maser sources.

This study is also dedicated to the analysis of the kinematics of the currently largest sample of Galactic masers, which is described in the Data section. Here we attempt to jointly determine the rotation curve of the young disk and the systematic deviations from it caused by the perturbations due to the spiral density wave. We use the method of statistical parallax to refine the maser distance scale. To solve this problem, we propose a new method for describing the field of space velocities, which allows the radial variation of the velocity ellipsoid axes and the exponential scale of the disk to be estimated.

2 DATA

We use published data for maser sources associated with very young stars located in star-forming regions. Currently, high-precision astrometric VLBI measurements have been performed by several research teams for more than one hundred such objects, yielding trigonometric parallaxes and proper motions with errors that on the average are no greater than 10% and 1 mas/yr, respectively.

One of such observational campaigns is the Japanese project VERA (VLBI Exploration of Radio Astrometry) targeting water (H_2O) Galactic masers (Hirota et al. 2007)

and SiO masers – which are very rarely found among young objects – (Kim et al. 2008), at 22 and 43 GHz, respectively.

Water and methanol (CH_3OH) masers are observed in the USA (VLBA) at 22 GHz and 12 GHz, respectively (Reid et al. 2009). Methanol masers are also observed in the framework of the European VLBI network (Rygl et al. 2010). These two projects are now parts of the combined BeSSeL program ¹ (Bar and Spiral Structure Legacy Survey, Brunthaler et al. (2011)).

Radio stars are observed with VLBI in the continuum at 8.4 GHz (Torres et al. 2007; Dzib et al. 2011) for the same purpose. In the framework of this program, radio sources in the Local arm are observed that are mostly associated with low-mass protostars ².

The number of measured masers is rapidly increasing. The first list of trigonometric-parallax, proper-motion, and radial-velocity measurements contained the data for 18 sources (Reid et al. 2009).

An analysis of this sample yielded a fairly large value of the circular rotation speed, $V_0 \sim 250$ km/s, and a noticeable lag in circular rotation of star-forming regions (~ 15 km/s) (Reid et al. 2009, Baba et al. 2009, Bovy et al. 2012, McMillan & Binney 2010). The influence of the spiral density wave, especially visible in the radial velocities V_R has been found for a sample of 28 masers (Bobylev and Bajkova 2010).

Honma et al. (2012) determined the fundamental parameters of the Galaxy based on the data for 52 masers.

The most recent “general” review of astrometric measurements provides the data for 103 masers (Reid et al. 2014). It was followed by a number of publications by the same authors dedicated to the analysis of masers located in individual spiral arms of the Galaxy with refined parameters reported for some of the masers. Wu et al. (2014) studied the Carina–Sagittarius arm (18 sources); Choi et al. (2014), the Perseus arm (25 sources); Sato et al. (2014), the Scutum arm (16 sources); Hachisuka et al. (2015), the Outer arm (five sources), and Sanna et al. (2014), the inner region of the Galaxy (six sources). Somewhat earlier, Xu et al. (2013) published their investigation of the Local arm (30 sources).

We supplemented the list of Reid et al. (2014) with the results of 40 recent astrometric measurements, thereby increasing the sample of masers with complete kinematic data to 136 sources. The references are given in Table 5 of the Appendix.

3 THE METHOD

3.1 Basic ideas

Wilson et al. (1991) were the first to use the method of statistical parallax to study the kinematics of Galactic disk objects: they applied it to analyze the velocity field and constrain the zero point of the photometric distance scale of classical Cepheids based on the PL relation. This was made possible by the publication of the list of the then best Cepheid proper motions compiled by Karimova & Pavlovskaya (1981). However, the results of

¹ <http://www3.mpifr-bonn.mpg.de/staff/abrunthaler/BeSSeL/index.shtml>

² <http://www.crya.unam.mx/~l.oinard/Gould/>

Wilson et al. (1991) were not very accurate and in some aspects not too realistic (e.g., extremely low, almost negligible vertical velocity dispersion of about 2 km/s) due to the small size of the sample (90 Cepheids) and rather large proper-motion errors. The first post-Hipparcos statistical-parallax study of Galactic-disk objects was performed by Luri et al. (1998), who also used it to constrain the zero point of the Cepheid distance scale. However, the above authors did not try to analyze the kinematics of their Cepheid sample and used a priori fixed values for Oort's constants and the Sun's Galactocentric distance. The first bona fide post-Hipparcos statistical-parallax study of Galactic disk objects combining both the analysis of the velocity field and refinement of the distance-scale zero point of classical Cepheids and young open clusters was performed by Rastorguev et al. (1999). It was followed by a statistical-parallax analysis of OB-associations (Dambis et al. 2001a), early-type supergiants (Dambis et al. 2001b), and a mixed sample of various young luminous objects (Zabolotskikh et al. 2002).

In this study we describe the scatter of the difference between the computed space velocity of an object, based on adopted distance, and its model value by the matrix of covariances, which is determined by random errors of observational data (heliocentric distances, radial velocities, and proper motions), velocity dispersion of the sample considered, and errors of model velocities induced by random and systematic errors of heliocentric distances. This approach, which allows the maximum-likelihood method to be used to determine the kinematical parameters, was first proposed and briefly described by Murray (1983). For detailed step-by-step instructions see the electronic tutorial by Rastorguev (2002) and papers by Hawley et al. (1986) and Dambis (2009). We present the basic ideas of the method in Sections 3.2 – 3.5.

Given the large spatial extent of our sample we have to take into account the variation of the parameters of the velocity ellipsoid with Galactocentric distance. The ratio of the two axes of the velocity ellipsoid parallel to the Galactic midplane obeys the following Lindblad relation:

$$\frac{\sigma V(R)}{\sigma U(R)} = \sqrt{1 + \frac{R}{2\omega} \cdot \frac{d\omega}{dR}}. \quad (1)$$

The thickness of the young disk varies little with Galactocentric distance and therefore it is safe to assume, to a good first approximation, that

$$\sigma W(R) = \sigma W(R_0) = \sigma W_0 = const.$$

It only remains for us to decide how the radial velocity dispersion of our maser sample may vary with Galactocentric distance. We proceed from the results of numerical simulations of the dynamical evolution of galaxy disks performed by Khoperskov et al. (2003). The above authors showed that an initially cool galactic disk rapidly reaches the state of marginal stability where radial velocity dispersion reaches its limit value in accordance with the criterion of Toomre (1964). Note that Saburova and Zasov (2014) used the marginal stability assumption to estimate the masses of galaxy disks.

The criterion of marginal stability written as

$$\frac{\kappa(R) \cdot \sigma U(R)}{\Sigma(R)} > 3.36 G$$

should apply to the radial velocity dispersion of intermediate-age stars, which are the main contributors to the surface density of the disk. Needless to say it is greater than the velocity dispersion of the youngest objects including Galactic masers.

As case **(A)**, we further assume, that local velocity dispersions of objects of different ages are proportional to each other and to the surface density of the disk. Hence the condition

$$\frac{\kappa(R) \cdot \sigma U(R)}{\Sigma(R)} \approx const (< 3.36 G),$$

where $\kappa(R)$ is the current epicyclic frequency; $\Sigma(R)$, the surface density of the disk, and G , the gravitational constant, implies the following relation between the current values of these parameters at Galactocentric distance R and the corresponding local values in the solar neighborhood (at the Galactocentric distance R_0):

$$\frac{\sigma U(R)}{\sigma U(R_0)} \approx \frac{\kappa(R_0)}{\kappa(R)} \cdot \exp\left(\frac{R_0 - R}{H_D}\right), \quad (2)$$

where H_D is the exponential disk scale. Hence our proposed first method of the description of the variation of radial velocity dispersion with the Galactocentric distance makes it possible to independently estimate the exponential disk scale H_D from kinematical data. Condition (2) can be treated as some kind of “equation of state” for the sample of objects under consideration.

In addition, we also examined two other cases of behavior of the radial velocity dispersion: **(B)** proportionality of radial velocity dispersion to the surface density of an exponential disk,

$$\frac{\sigma U(R)}{\sigma U(R_0)} \approx \exp\left(\frac{R_0 - R}{H_D}\right), \quad (3)$$

and **(C)** constancy of radial velocity dispersion, i.e. $\sigma U(R) = \sigma U(R_0) = \sigma U_0 = const$.

3.2 Kinematic models

In this paper we consider two kinematical models. The first model includes only differential rotation of the Galaxy with angular velocity $\omega(R)$ and solar motion relative to the local sample:

$$\begin{pmatrix} V_r \\ kr\mu_l \\ kr\mu_b \end{pmatrix} - \begin{pmatrix} R_0(\omega - \omega_0) \sin l \cos b \\ (R_0 \cos l - r \cos b)(\omega - \omega_0) - r\omega_0 \cos b \\ -R_0(\omega - \omega_0) \sin l \sin b \end{pmatrix} - G^T \times \begin{pmatrix} U_0 \\ V_0 \\ W_0 \end{pmatrix} = \delta \vec{V}_{loc}, \quad (4)$$

where V_r is the line-of-sight velocity; $k = 4.741$ km/s/kpc/(mas/yr); r , the adopted heliocentric distance of the object (in kpc), $(\mu_l \mu_b)$, the components of proper motion along Galactic coordinates (in mas/yr), and $(U_0 V_0 W_0)$, the components of the velocity of the local sample relative to the Sun, and T denotes transposition.

The rotation matrix G

$$G = \begin{pmatrix} \cos b \cos l & -\sin l & -\sin b \cos l \\ \cos b \sin l & \cos l & -\sin b \sin l \\ \sin b & 0 & \cos b \end{pmatrix} \quad (5)$$

4 Milky Way masers

transforms the components of the velocity of the object

$$\vec{V}_{loc} = \begin{pmatrix} V_r \\ kr \mu_l \\ kr \mu_b \end{pmatrix}, \quad (6)$$

given in the local coordinate system (associated with the direction to the object) into the velocity components

$$\vec{V}_{gal} = \begin{pmatrix} U \\ V \\ W \end{pmatrix} = G \times \vec{V}_{loc}$$

in heliocentric Cartesian coordinate system $(x y z)$ with the origin at the Sun, the x -axis pointing to the Galactic center and the z -axis pointing to the North Galactic pole.

The second model also includes the contribution of non-circular motions induced by the spiral density wave and computed in linear approximation:

$$\begin{aligned} & \begin{pmatrix} V_r \\ kr \mu_l \\ kr \mu_b \end{pmatrix} - \begin{pmatrix} R_0(\Omega - \Omega_0) \sin l \cos b \\ (R_0 \cos l - r \cos b)(\Omega - \Omega_0) - r\Omega_0 \cos b \\ -R_0(\Omega - \Omega_0) \sin l \sin b \end{pmatrix} - \\ & - \begin{pmatrix} -(R_0(\frac{\Pi}{R} - \frac{\Pi_0}{R_0}) \cos l - \frac{\Pi}{R} r \cos b) \cos b \\ R_0(\frac{\Pi}{R} - \frac{\Pi_0}{R_0}) \sin l \\ (R_0(\frac{\Pi}{R} - \frac{\Pi_0}{R_0}) \cos l - \frac{\Pi}{R} r \cos b) \sin b \end{pmatrix} - \\ & - G^T \times \begin{pmatrix} U_0 \\ V_0 \\ W_0 \end{pmatrix} = \delta \vec{V}_{loc}, \end{aligned} \quad (7)$$

where R and R_0 are the Galactocentric distances of the object and the Sun, respectively; Π and Π_0 , the radial perturbations of the velocity of the object and the Sun, respectively. Here modified angular velocities

$$\Omega = \omega + \frac{\Theta}{R}, \quad \Omega_0 = \omega_0 + \frac{\Theta_0}{R_0}, \quad (8)$$

include tangential velocity perturbations of the object and the Sun, respectively, and $\Pi, \Pi_0, \Theta, \Theta_0$ are given by (21).

In both models (4,7) the difference $\delta \vec{V}_{loc}$ between the observed and model velocities is a random vector whose matrix of covariances is given in Section 3.3.

3.3 Matrix of covariances

The maximum-likelihood method used in this study allows one to determine not only the main kinematical properties of the sample, but also infer the systematic correction to the underlying distance scale of objects (Murray 1983, Hawley et al. 1986, Rastorguev 2002, Dambis 2009). We further assume that the true distance r_t is related to the adopted distance r as $r_t = r/P$, where P is the distance-scale correction factor.

The full matrix of covariances of vector \vec{V}_{loc} includes errors of observational data; ‘‘cosmic’’ dispersion (three-dimensional distribution of residual velocities), and errors of the model velocity field induced by random and systematic errors of the adopted distances (Rastorguev 2002):

$$L_{loc} = L_{err} + L_{resid} + \delta L \quad (9)$$

The observed local vector of velocity errors at the adopted distance r is given by the formula

$$\delta \vec{V}_{loc} = \begin{pmatrix} \delta V_r \\ kr \delta \mu_l \\ kr \delta \mu_b \end{pmatrix}, \quad (10)$$

and therefore in the absence of correlations between the errors of line-of-sight velocities and those of proper-motion components (which is the case for the sample of maser sources considered), the matrix of observational errors has the form

$$\begin{aligned} L_{err} &= \langle \delta \vec{V}_{loc} \cdot \delta \vec{V}_{loc}^T \rangle = \\ &= \begin{pmatrix} \sigma_{V_r}^2 & 0 & 0 \\ 0 & k^2 r^2 \sigma_{\mu_l}^2 & k^2 r^2 \sigma_{\mu_l} \sigma_{\mu_b} \rho_{\mu_l \mu_b} \\ 0 & k^2 r^2 \sigma_{\mu_l} \sigma_{\mu_b} \rho_{\mu_l \mu_b} & k^2 r^2 \sigma_{\mu_b}^2 \end{pmatrix}, \end{aligned} \quad (11)$$

where angle brackets denote averaging over the ensemble of objects in the given region and $\rho_{\mu_l \mu_b}$ is the correlation coefficient of proper motion components.

Note: Data on maser sources are given in equatorial coordinate system, with no correlations of proper motion components. To simplify calculations, we first evaluate the matrix of covariances L_{err} in the equatorial coordinate system and then use standard rotation transformation to transform the matrix of covariances to the galactic coordinate system.

Let us now introduce two auxiliary matrices:

$$P = \begin{pmatrix} 1 & 0 & 0 \\ 0 & p & 0 \\ 0 & 0 & p \end{pmatrix}$$

and

$$M = \begin{pmatrix} 0 & 0 & 0 \\ 0 & 1 & 0 \\ 0 & 0 & 1 \end{pmatrix}$$

It is easy to understand that the first matrix relates the components of space velocity \vec{V}_{loc} computed for the adopted heliocentric distances r to the corresponding quantities computed from the true heliocentric distances r_t of objects.

We compute the matrix of covariances L_{resid} that is responsible for the intrinsic scatter of stellar velocities in the Galaxy, which is usually described by the three-dimensional Gaussian distribution with the principal axes $(\sigma U \sigma V \sigma W)$, assuming, to a first approximation, that the $(\sigma U \sigma V)$ axes are parallel to the Galactic midplane with the major axis directed toward the Galactic center. We take into account the inclination of the velocity ellipsoid in the region of the Galaxy where we observe the object to the line of sight. To this end we introduce the auxiliary angle φ that determines the orientation of the velocity ellipsoid and which is equal to the angle between the projection of the line of sight onto the Galactic plane and the projection of the major axis of the velocity ellipsoid. It can be easily shown that this angle is given by the following formula

$$\tan \varphi = \frac{R_0 \cdot \sin l}{R_0 \cdot \cos l - r \cdot \cos b}.$$

The rotation matrix

$$G_S = \begin{pmatrix} \cos b \cos \varphi & \cos b \sin \varphi & \sin b \\ -\sin \varphi & \cos \varphi & 0 \\ -\sin b \cos \varphi & -\sin b \sin \varphi & \cos b \end{pmatrix} \quad (12)$$

determines the transformation from the coordinate system connected with the axes of the velocity ellipsoid to the local coordinate system connected with the direction to the object. In the coordinate system determined by the principal

axes of the velocity ellipsoid the matrix of covariances has the following diagonal form

$$L_0 = \begin{pmatrix} \sigma U^2 & 0 & 0 \\ 0 & \sigma V^2 & 0 \\ 0 & 0 & \sigma W^2 \end{pmatrix}. \quad (13)$$

When going to the local coordinate system it transforms in accordance with the following well-known formula:

$$L_{resid} = G_S \times L_0 \times G_S^T. \quad (14)$$

Given the systematic correction to the adopted distance scale the matrix of covariances L_{resid} acquires the following final form

$$L_{resid} = P \times G_S \times L_0 \times G_S^T \times P^T. \quad (15)$$

The smallest contribution to covariance matrix is provided by the third term, which is proportional to the squared random error of the distance scale. This term includes the systematic velocity, its derivative with respect to heliocentric distance, and the matrix of ‘‘cosmic’’ dispersion:

$$\delta L = (\sigma_\pi/\pi)^2 \cdot [M \times G_S \times L_0 \times G_S^T \times M^T + \tilde{\Upsilon} \cdot \tilde{\Upsilon}^T], \quad (16)$$

where to simplify the formulas we introduce the following auxiliary vector

$$\tilde{\Upsilon} = M \times [G^T \times \vec{V}_0 + \vec{V}_{sys}] - r/p \cdot P \times \partial \vec{V}_{sys}/\partial r.$$

Here

$$\vec{V}_0 = \begin{pmatrix} U_0 \\ V_0 \\ W_0 \end{pmatrix} \quad (17)$$

is the the velocity of the sample of objects relative to the Sun and

$$\vec{V}_{sys} = \vec{V}_{rot} + \vec{V}_{spir} \quad (18)$$

is the full velocity of systematic motions including the differential rotation of the disk and perturbations from the spiral pattern. Note that all components of the full matrix of covariances L_{loc} are computed using the adopted heliocentric distances to the objects.

3.4 Systemic velocity field

In our models we describe purely circular motions (the differential rotation of the disk) via polynomial expansion of the difference of angular velocities as a function of Galactocentric distance in the following form

$$(\omega - \omega_0) \approx \sum_{n=1}^M \frac{1}{n!} \frac{\partial^n \omega_0}{\partial r^n} \cdot (R - R_0)^n, \quad (19)$$

with the order of expansion M ranging from 4 to 5.

We describe the kinematical perturbations induced by the spiral density wave in terms of the linear theory (Lin and Shu 1964, Lin et al. 1969). The trailing spiral pattern is described by the following formula for the phase angle of the object relative to the density wave:

$$\chi - \chi_0 = m \cdot (\psi - \cot i \cdot \lg \frac{R}{R_0}). \quad (20)$$

Here χ_0 is the phase of the Sun; i , the pitch angle (it is negative for a trailing pattern); ψ , the Galactocentric position angle of the object counted from the direction to the Sun in the direction of the disk rotation, and m , the number of spiral arms. Hereafter we set $m = 4$ given serious arguments for the four-armed structure of the global spiral pattern provided by a number of recent studies of the spiral pattern of the Galaxy (Vallée 2013, Vallée 2014, Vallée 2015, Dambis et al. 2015).

The radial and tangential velocity perturbations can be written in terms of the perturbation amplitudes (f_R f_Θ) and phase angles as follows:

$$\begin{pmatrix} \Pi \\ \Theta \end{pmatrix} = \begin{pmatrix} f_R \cdot \cos \chi \\ f_\Theta \cdot \sin \chi \end{pmatrix}, \quad \begin{pmatrix} \Pi_0 \\ \Theta_0 \end{pmatrix} = \begin{pmatrix} f_R \cdot \cos \chi_0 \\ f_\Theta \cdot \sin \chi_0 \end{pmatrix} \quad (21)$$

where Π_0 and Θ_0 are, respectively, the radial and tangential perturbations for the Sun entering equations (7, 8). Here Π is positive in the direction out of the Galactic center.

Note again that when computing the kinematical parameters of the disk with the allowance for both the differential rotation and perturbations induced by the spiral pattern the terms describing differential rotation in the above formulas (the so-called Bottlinger equations) should be modified as $\omega \rightarrow \Omega = \omega + f_\Theta \cdot \sin \chi / R$, $\omega_0 \rightarrow \Omega_0 = \omega_0 + f_\Theta \cdot \sin \chi_0 / R_0$ (see also 8), in order to explicitly single out the tangential velocity component $f_\Theta \cdot \sin \chi / R$ associated with perturbations.

The formula for the matrix of covariances includes the partial derivatives of the contribution of systematic velocities with respect to heliocentric distance. The corresponding formula for differential rotation can be easily derived:

$$\frac{\partial \vec{V}_{rot}}{\partial r} = \begin{pmatrix} R_0 \cdot \frac{\partial}{\partial r} (\omega - \omega_0) \cdot \sin l \cdot \cos b \\ (R_0 \cdot \cos l - r \cdot \cos b) \cdot \frac{\partial}{\partial r} (\omega - \omega_0) - \omega \cdot \cos b \\ -R_0 \cdot \frac{\partial}{\partial r} (\omega - \omega_0) \cdot \sin l \cdot \sin b \end{pmatrix}, \quad (22)$$

where the partial derivative of the difference of angular velocities is equal to

$$\begin{aligned} \frac{\partial (\omega - \omega_0)}{\partial r} &\approx \frac{\cos b}{R} \cdot (r \cos b - R_0 \cos l) \times \\ &\times \sum_{n=1}^M \frac{1}{(n-1)!} \frac{\partial^n \omega_0}{\partial r^n} \cdot (R - R_0)^{n-1}, \end{aligned} \quad (23)$$

and M is the order of expansion of the angular velocity into a Taylor series.

The formula for the partial derivative of the contribution of the spiral pattern to the velocity field is somewhat more complex. We first write simpler formulas for D , derivatives of Galactocentric distance R , position angle ψ , and phase angle χ :

$$D = R_0 \cos l - r \cos b.$$

$$\frac{\partial R}{\partial r} = -D/R \cos b$$

$$\frac{\partial \psi}{\partial r} = R_0/R^2 \cos b \sin l$$

$$\frac{\partial \chi}{\partial r} = m \cdot \left(\frac{\partial \psi}{\partial r} - \frac{\partial R}{\partial r} \cdot \cot i / R \right) \quad (24)$$

The general formula for the column vector of the partial derivative

6 Milky Way masers

$$\frac{\partial \vec{V}_{spir}}{\partial r} = \left(\frac{\partial V_r^{sp}}{\partial r} \quad \frac{\partial V_l^{sp}}{\partial r} \quad \frac{\partial V_b^{sp}}{\partial r} \right)^T \quad (25)$$

is too unwieldy to write and therefore we give the separate formulas for its three components (line-of-sight velocities V_r , tangential velocities along Galactic longitude and latitude V_l , V_b).

$$\begin{aligned} \frac{\partial V_r^{sp}}{\partial r} &= f_R/R \cdot \cos b \cdot (\cos b \cos \chi + \\ &+ D \cdot (\cos \chi \cdot \frac{\partial R}{\partial r}/R + \sin \chi \cdot \frac{\partial \chi}{\partial r})) - \\ &- f_\Theta R_0/R \cdot \sin l \cos b \cdot (\cos \chi \cdot \frac{\partial \chi}{\partial r} - \sin \chi \cdot \frac{\partial R}{\partial r}/R); \\ \frac{\partial V_l^{sp}}{\partial r} &= -f_R R_0/R \cdot (\sin \chi \cdot \frac{\partial \chi}{\partial r} + \cos \chi \cdot \frac{\partial R}{\partial r}/R) \cdot \sin l + \\ &+ f_\Theta/R \cdot (\cos b \sin \chi + D \cdot (\sin \chi \cdot \frac{\partial R}{\partial r}/R - \cos \chi \cdot \frac{\partial \chi}{\partial r})); \\ \frac{\partial V_b^{sp}}{\partial r} &= -\frac{\partial V_r^{sp}}{\partial r} \cdot \tan b. \end{aligned}$$

3.5 Distribution of residual velocities and the Likelihood Function

The three-dimensional probability function of the distribution of residual velocities – the difference between the observed and model velocities of the star, $\delta \vec{V}_{loc}$ – can be written in the following general form Murray (1983)

$$\begin{aligned} f(\delta \vec{V}_{loc} | \Lambda) &= \\ &= (2\pi)^{-3/2} \cdot |L_{loc}|^{-1/2} \cdot \exp\left\{-\frac{1}{2} \cdot \delta \vec{V}_{loc}^T \times L_{loc}^{-1} \times \delta \vec{V}_{loc}\right\}, \end{aligned}$$

where Λ is the set of unknown parameters of the problem that describe the model velocity field; $|L_{loc}|$ and L_{loc}^{-1} are the determinant and inverse of the matrix of covariances L_{loc} (9), respectively, computed individually for each object of the sample. Note that the matrix of covariances also depends on the parameter vector Λ . The distribution function has the meaning of the probability density for the residual velocity of a particular star. Because stars are distributed independently of each other in the velocity space, their N-point distribution function is equal to the product of functions $f_i(\delta \vec{V}_{loc} | \Lambda)$ for all stars of the sample:

$$F(\delta \vec{V}_{loc}(1), \dots, \delta \vec{V}_{loc}(N) | \Lambda) = \prod_{i=1}^N f_i(\delta \vec{V}_{loc} | \Lambda), \quad (26)$$

where N is the number of objects. The gist of the maximum-likelihood method is that the real (i.e., the actual) distribution of the velocities of the objects of our sample is assumed to be the most probable among all possible distributions. Hence the parameter vector Λ (which in addition to the parameters of the kinematical model includes the quantity P , the distance-scale correction factor) responsible for the probability density f of residual velocities should be chosen so as to *maximize* the probability $F(\Lambda)$ for the actual sample. This problem is usually solved by minimizing the logarithm of the N-particle probability density F with the sign reversed, i.e., the so-called *likelihood function*

$$LF(\Lambda) = -\ln F(\delta \vec{V}_{loc}(1), \dots, \delta \vec{V}_{loc}(N) | \Lambda) =$$

$$-\sum_{i=1}^N \ln f(\delta \vec{V}_{loc}(i) | \Lambda)$$

and reducing the problem to the standard search for the *minimum of the likelihood function* $LF(\Lambda)$ using one of the efficient *multidimensional optimization* algorithms. We now substitute into the above formula the formula for probability density $f(\delta \vec{V}_{loc}(i) | \Lambda)$ to derive the following explicit formula for the likelihood function:

$$\begin{aligned} LF(\Lambda) &= \frac{3}{2}N \cdot \ln 2\pi + \\ &+ \frac{1}{2} \sum_{i=1}^N [\ln |L_{loc}(i)| + \delta \vec{V}_{loc}^T(i) \times L_{loc}(i)^{-1} \times \delta \vec{V}_{loc}(i)], \quad (27) \end{aligned}$$

where i -th covariation matrix $L_{loc}(i)$ is given by (9), space velocity vector $\delta \vec{V}_{loc}(i)$ is given by (4) or (7) and summation is performed over index i denoting the current object of the sample.

3.6 Calculation of errors

Probability function $LF(\Lambda)$ is a complicated nonlinear function of the unknown kinematical parameters and the distance-scale correction factor. In the vicinity of the global minimum it can be approximated rather well by a multidimensional quadratic function of all variables (many optimization methods are based on such a representation of the target function). Strictly speaking, the confidence intervals for the unknown kinematical parameters (i.e., their root-mean-squared errors) can be determined by projecting the section of the likelihood function profile by the hypersurface $LF(\Lambda) = LF_0 + 1$ (here LF_0 is the minimum value of the likelihood function reached in the process of solution) onto the axes corresponding to parameters Λ (Press et al. 2007). With this, we can estimate not only the errors of parameters determined but also their correlations (see Figs. 2 and 3 as examples). The errors shown in the Tables 1 – 4 were estimated by this technique.

4 RESULTS

4.1 Kinematic parameters of the Milky Way young disk

We performed all our computations for masers with Galactocentric distances greater than 3 kpc to reduce the effect of the Galactic bar on the inferred kinematics of the sample (Chemin et al. 2015). We further excluded from the initial list of maser sources three objects whose (formally precise) observed velocities differ from the corresponding model velocities by more than 3σ . The final sample consists of 131 maser sources. The results are listed in the Tables 1 – 4, where minimal values of the likelihood functions, LF_{min} , are also shown for all sets of calculations.

Tables 1 – 4 list the inferred kinematical parameters and their standard errors for four models: A1, A2, C1 and C2. Model A1 includes differential rotation and spiral perturbations (7), whereas Model A2 includes only differential rotation (4); both use Toomre-like “equation of state” (2), i.e. dependence of radial velocity dispersion on Galactocentric distance and disk surface density. Our analysis of maser

Table 1. Solution for N = 131 maser sample (with Galactocentric distance $R \geq 3$ kpc). **Model A1:** circular rotation and spiral-wave perturbations (four arms) with 4th-order expansion of the Galactic rotation curve.

P	R_0 kpc	H_D kpc	U_0 km/s	V_0 km/s	W_0 km/s	σU_0 km/s	σW_0 km/s		
0.979 ± 0.018	8.21 ± 0.12	4.31 ± 0.90	-11.06 ± 1.31	-18.26 ± 1.19	-8.76 ± 1.06	10.02 ± 0.90	5.74 ± 0.75		
f_R km/s	f_Θ km/s	χ_0 deg.	i deg.	ω_0 km/s/kpc	$d\omega/dR$ km/s/kpc ²	$d^2\omega/dR^2$ km/s/kpc ³	$d^3\omega/dR^3$ km/s/kpc ⁴	$d^4\omega/dR^4$ km/s/kpc ⁵	LF_{min}
-6.80 ± 1.37	+3.10 ± 0.95	123.1 ± 10.1	-10.44 ± 0.29	28.94 ± 0.51	-3.91 ± 0.07	0.86 ± 0.03	0.01 ± 0.03	-0.08 ± 0.10	1085.7870

Table 2. **Model A2:** purely circular rotation and fixed scale coefficient $p = 1.00$ (5th-order expansion of the Galactic rotation curve).

P	R_0 kpc	H_D kpc	U_0 km/s	V_0 km/s	W_0 km/s	σU_0 km/s	σW_0 km/s		
1.00	8.31 ± 0.13	4.34 ± 0.75	-7.73 ± 1.52	-17.69 ± 1.20	-8.64 ± 0.91	11.59 ± 0.95	5.65 ± 0.80		
ω_0 km/s/kpc	$d\omega/dR$ km/s/kpc ²	$d^2\omega/dR^2$ km/s/kpc ³	$d^3\omega/dR^3$ km/s/kpc ⁴	$d^4\omega/dR^4$ km/s/kpc ⁵	$d^5\omega/dR^5$ km/s/kpc ⁶	LF_{min}			
29.03 ± 0.52	-3.94 ± 0.08	1.13 ± 0.07	-0.06 ± 0.11	-0.30 ± 0.02	0.14 ± 0.02	1465.8692			

Table 3. **Model C1:** circular rotation and spiral-wave perturbations (four arms) with 4th-order expansion of the Galactic rotation curve and constant velocity dispersions σU and σW .

P	R_0 kpc	U_0 kpc	V_0 km/s	W_0 km/s	σU_0 km/s	σW_0 km/s			
0.961 ± 0.020	8.27 ± 0.13	-10.98 ± 1.40	-19.62 ± 1.15	-8.93 ± 1.05	9.43 ± 0.88	5.86 ± 0.80			
f_R km/s	f_Θ km/s	χ_0 deg.	i deg.	ω_0 km/s/kpc	$d\omega/dR$ km/s/kpc ²	$d^2\omega/dR^2$ km/s/kpc ³	$d^3\omega/dR^3$ km/s/kpc ⁴	$d^4\omega/dR^4$ km/s/kpc ⁵	LF_{min}
-7.00 ± 1.48	2.62 ± 1.05	130.3 ± 10.8	-10.39 ± 0.25	28.35 ± 0.45	-3.83 ± 0.08	1.17 ± 0.05	-0.08 ± 0.04	-0.30 ± 0.03	1079.2939

Table 4. **Model C2:** purely circular rotation with fixed scale coefficient ($p = 1.00$), 5th-order expansion of the Galactic rotation curve and constant velocity dispersions σU and σW .

P	R_0 kpc	U_0 km/s	V_0 km/s	W_0 km/s	σU_0 km/s	σW_0 km/s			
1.00	8.19 ± 0.12	-7.57 ± 1.55	-18.17 ± 1.20	-8.64 ± 0.92	10.87 ± 0.91	5.65 ± 0.80			
ω_0 km/s/kpc	$d\omega/dR$ km/s/kpc ²	$d^2\omega/dR^2$ km/s/kpc ³	$d^3\omega/dR^3$ km/s/kpc ⁴	$d^4\omega/dR^4$ km/s/kpc ⁵	$d^5\omega/dR^5$ km/s/kpc ⁶	LF_{min}			
28.64 ± 0.53	-4.00 ± 0.09	1.28 ± 0.04	-0.10 ± 0.02	-0.37 ± 0.02	0.19 ± 0.02	1463.7012			

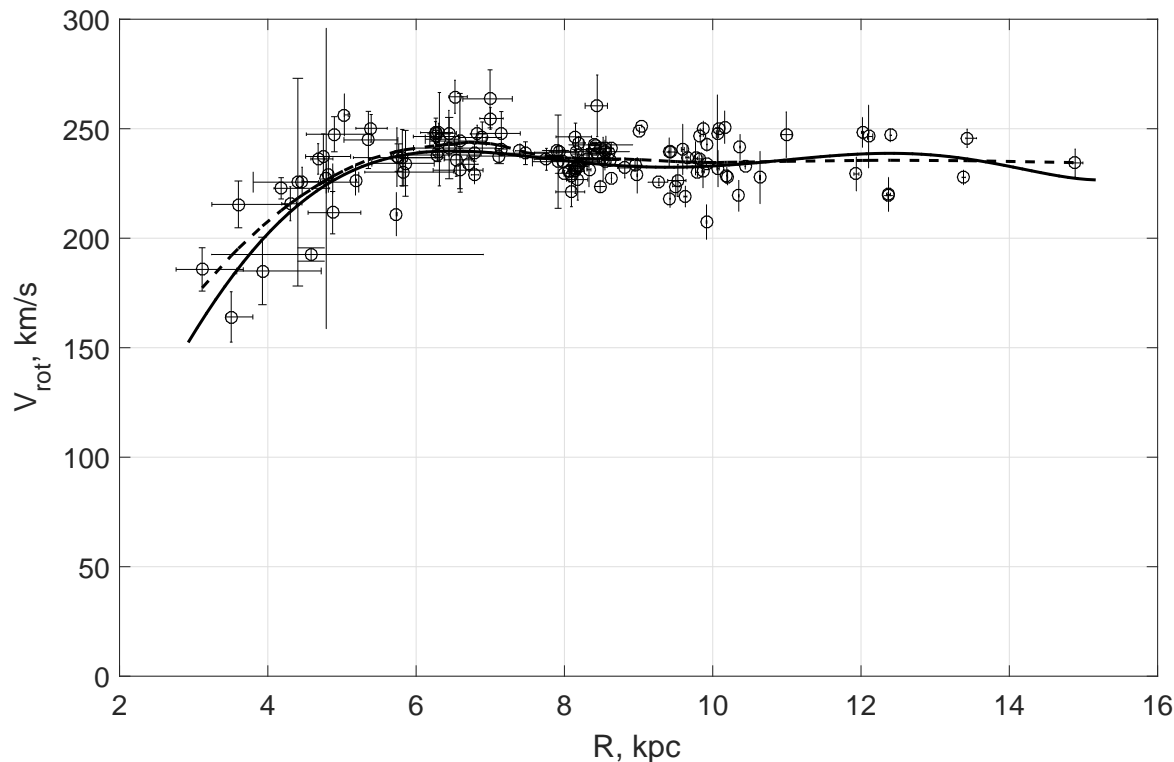


Figure 1. Rotation curve of the Galactic disk. The solid line shows the fit obtained by expanding angular velocity into a 4th-order series in the distance difference (Model C1). Also plotted are the tangential velocities of individual masers and their standard errors computed based on the heliocentric distances, radial velocities, and proper motions of the masers and the velocity of the Sun inferred in this paper, as well as distance errors computed based on parallaxes. The dashed line shows the smoothed dependence of tangential velocities on Galactocentric distance computed using the second-order locally weighted scatterplot smoothing method (LOESS).

data in terms of these models yields an exponential disk scale of be $H_D \approx (4.3 \pm 0.9)$ kpc.

Models B1 and B2 are similar to A1 and A2, respectively, but use simple exponential dependence of radial velocity dispersion on Galactocentric distance (3). These models imply the disk exponential scales of $H_D \approx 18_{-10}^{+60}$ kpc and $H_D \approx 16_{-6}^{+30}$ kpc, respectively. All other parameters agree very well with those given by Models C1 and C2. As we see from the analysis of errors, the likelihood function (LF) profile along the H_D axis near LF_{min} is expected to be very asymmetric, with a long “tail” extending to very large values of H_D . For this reason, we do not present here these results.

We therefore decided to calculate a set of models C1 and C2, similar to A1 and A2, respectively, but with $\sigma U(R) = \sigma U_0 = const$, i.e. with formally infinite values of the disc scale, H_D , in (3). The corresponding model parameters are listed in Tables 3 and 4. Systematically slightly lower values of LF_{min} for C1 and C2 with respect to A1 and A2 (by 6 and 2 units, respectively), indicate that Models C1 and C2 with constant velocity dispersion along Galactocentric radius provide better fits to observations with respect compared to the model with variable σU .

Figure 1 shows the rotation curve of the population of maser sources. It remains practically flat over the interval from 5-6 to 15 kpc with a small depression at about 9 kpc and small variations over ~ 1 kpc scale lengths, which are

most likely due to spiral perturbations (see also Fig. 4). The computed rotation velocity at Solar distance is of about $V_0 \approx (235 - 238)$ km/s ± 7 km/s.

Some of the parameters incorporated into our models of the velocity field are mutually correlated. Figures 2 and 3 show the (R_0, P) and (R_0, ω_0) two-parameter scattering ellipses, respectively. It is easy to understand that R_0 also correlates with the derivative of angular velocity, $(d\omega/dR)_0$, and radial velocity dispersion, σU_0 .

Figure 4 shows the residuals of the radial, Δ_{VR} , tangential, Δ_{VT} , and vertical, Δ_{VZ} , velocity components from the model of purely circular motions. Large quasi-periodic variations of radial velocity, Δ_{VR} , are immediately apparent, which are due to perturbations produced by the spiral pattern. The Δ_{VT} residuals also show similar but not so evident variations. Similar behaviour of vertical component, Δ_{VZ} , was first noted by Bobylev and Bajkova (2015).

Models A1 and C1 provide very reliable estimates of the parameters responsible for velocity perturbations induced by the spiral density wave. Both the mean radial and tangential perturbation amplitudes are significant and estimated as $f_R \approx (-6.9 \pm 1.4)$ km/s and $f_\theta \approx (+2.8 \pm 1.0)$ km/s, respectively. The mean phase angle of the Sun relative to the ridge of spiral density wave is close to $(125^\circ \pm 10)^\circ$, and the estimates of the pitch angle are very stable and accurate: $i \approx (-10.4 \pm 0.3)^\circ$. The adequateness of the description of the spiral pattern is additionally confirmed by very substan-

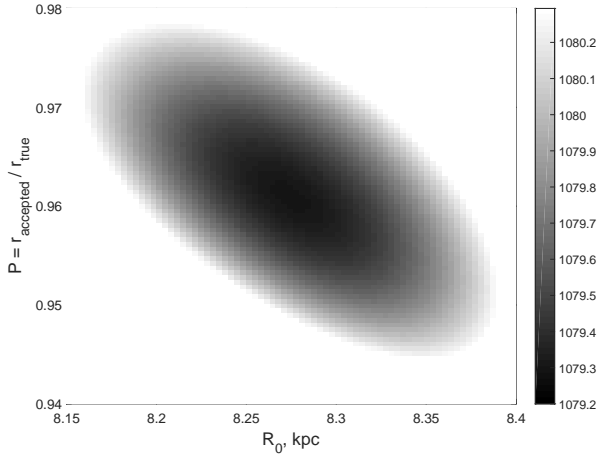


Figure 2. Cross section of the likelihood function by the hyper-surface $LF = LF_0 + 1$ near the global minimum: projection onto the R_0 and P axes (Model C1).

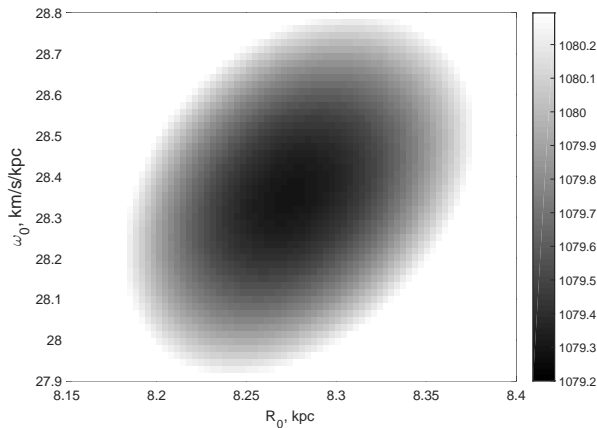


Figure 3. Cross section of the likelihood function by the hyper-surface $LF = LF_0 + 1$ near the global minimum: projection onto the R_0 and ω_0 axes (Model C1).

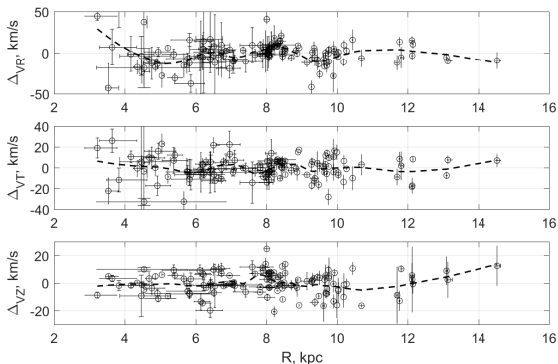


Figure 4. Residual deviations of the components of maser space velocities (Δ_{VR} , Δ_{VT} , Δ_{VZ}) from the Model C2 of purely circular rotation.

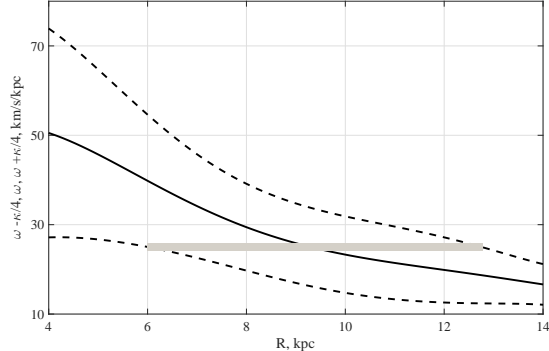


Figure 5. Resonance diagram for the sample of Galactic masers computed for the four-armed spiral pattern. The solid line shows the Galactocentric distance dependence of the angular velocity of disk rotation $\omega(R)$; the dashed lines show the positions of the Lindblad resonances (the upper and lower curves correspond to the outer $(\omega(R) + \kappa(R)/4)$ and inner $(\omega(R) - \kappa(R)/4)$ resonances, respectively). The gray strip corresponds to the pattern speed $\Omega_P \approx 25$ km/s/kpc (Dambis et al. 2015).

tial reduction of LF_{min} value (by approximately 380 – 384 units) for Models A1 – C1 compared to Models A2 – C2, respectively, which take into account only pure rotation.

Our best Model C1 (Table 3) yields the estimates of radial and vertical velocity dispersion for extremely young stellar populations, $\sigma_{U0} \approx (9.4 \pm 0.9)$ km/s and $\sigma_{W0} \approx (5.9 \pm 0.8)$ km/s, which are less than the corresponding values for young populations, such as open star clusters and Cepheids (Rastorguev et al. 1999; Dambis et al. 2001b; Rastorguev et al. 2001; Zabolotskikh et al. 2002), and comparable to the results obtained for very young OB-associations (Dambis et al. 2001a; Melnik and Dambis 2009) and longest-periods Cepheids (Bobylyev 2016) based on GAIA Dr.1 data (Brown et al. 2016). Small values of the velocity dispersions, σ_U and σ_W , indicate that maser sources, which are the representatives of the “coolest” disk population, retain the dynamical properties of the interstellar medium. Consequently, the most likely “equation of state” of maser population means that radial and vertical velocity dispersions do not depend on Galactocentric distance.

Note again, that in our analysis of the kinematics of Galactic masers we for the first time took into account the variation of the shape of the velocity ellipsoid in accordance with the Lindblad theorem.

We used our rotation curve and computed the resonance diagram for four-armed spiral pattern (Fig. 5). This diagram demonstrates that a global four-armed spiral pattern can exist in the Galactocentric distance interval from 6 to 13 kpc with a corotation distance of about 9.5 - 10 kpc and a pattern speed of about 25 km/s/kpc (see, e.g., Dambis et al. (2015)).

Figure 6 shows the positions of maser sources and the four kinematic spiral arms determined in this study. Note the concentration of masers to the Perseus, Carina-Sagittarius, and Inner arms, and the small number of masers near the Outer arm. The inferred parameters of the spiral pattern – including the pitch angle and the phase of the Sun – agree well with recent results of Dambis et al. (2015) ob-

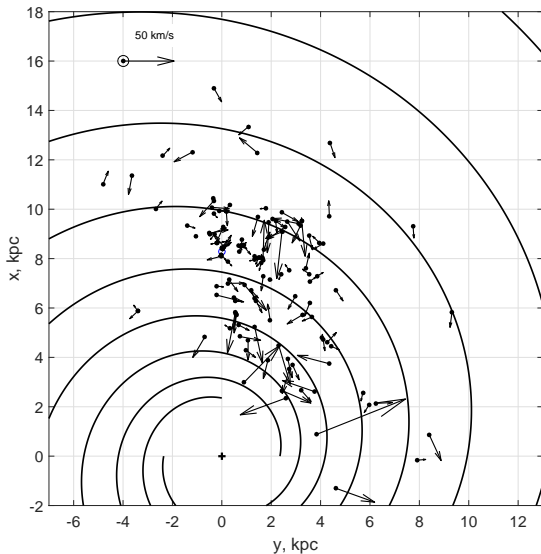


Figure 6. Kinematic spiral pattern and positions of the masers of the sample studied. The large pentagram shows the position of the Sun. The arrows show the deviations of the space velocities of objects from purely circular orbits. The scale vector at the top left corner corresponds to the velocity of 50 km/s.

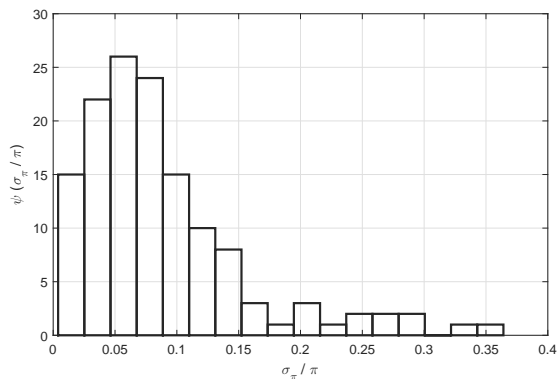


Figure 7. The distribution of relative errors of measured masers parallaxes.

tained by analyzing the space distribution of a large Cepheid sample.

4.2 Maser distance scale

First and foremost, we point out that the adjustment factor P for the scale of maser distances is close to unity for Models A1 and C1. We calculated the Lutz-Kelker bias for 5 different levels of relative errors of masers parallaxes, $\sigma_\pi/\pi = 0.04, 0.06, 0.08, 0.10, 0.12$, from modified standard expression (Lutz & Kelker 1973) that we adjusted to the case of flat distribution of stars (see Fig. 8):

$$F(P) \sim P^{-3} \exp\left[-\frac{(P-1)^2}{2(\sigma_\pi/\pi)^2}\right], \quad (28)$$

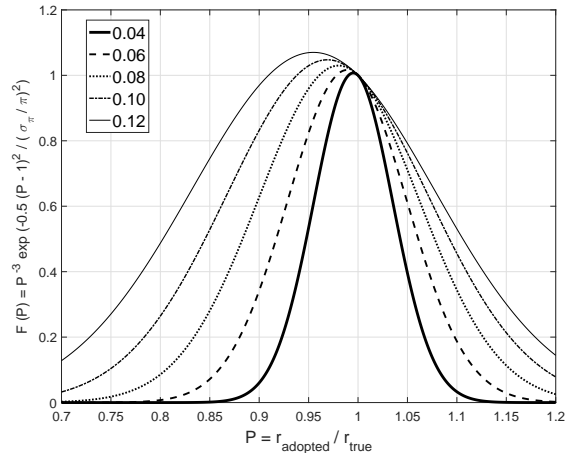


Figure 8. Lutz-Kelker bias $F(P)$ (28) calculated for different values of the relative parallax error, $\sigma_\pi/\pi = 0.04, 0.06, 0.08, 0.10, 0.12$, for flat stellar distribution. Our estimates of the distance scale coefficient $P \approx 0.98 \pm 0.02$ and 0.96 ± 0.02 (Models A1, C1) are fully consistent with the characteristic accuracy of maser parallaxes (see also Fig. 7), with the mean and median values of $\sigma_\pi/\pi \approx 0.09$ and 0.07 , respectively.)

where $P = r/r_t = r_{\text{adopted}}/r_{\text{true}}$. The systematic shift of the median and mean values of the distribution function $F(P)$ to the left can be explained by systematic under-estimation of distances calculated from parallax data. As can be seen, our estimates of the distance scale factor $P \approx 0.98 \pm 0.02$ and $P \approx 0.96 \pm 0.02$ (Models A1 and C1 respectively) agree well with the typical mean accuracy of maser parallaxes (see Fig. 7). Consequently, the scale of maser trigonometric parallaxes has no large systematic biases despite the fact that the mean fractional error of measured parallaxes is of about 5-7%. Considering this, we set $P = 1.00$ in Models A2 and C2.

All models, A1 – A2, C1 – C2 yield very close estimates for the Galactocentric distance of the Sun, R_0 , with the weighted mean value of $\langle R_0 \rangle \approx 8.24 \pm 0.12$ kpc, which agrees very well with the most recent determinations.

4.3 Disk scale estimate based on asymmetric drift law

Let us now obtain an independent estimate for the disk scale H_D for intermediate-age populations based on hydrodynamic equation of stellar dynamics, observational data about the asymmetric drift law in the local neighborhood (Dehnen and Binney 1998) and inferred rotation-curve parameters assuming that the radial velocity dispersion, $\sigma V(R)$, follows Toomre-like “equation of state” (2).

We first write the well-known formula for the asymmetric drift in axisymmetric stellar systems with small dispersion of residual velocities:

$$\Delta\Theta = \Theta_c - \Theta_0 \approx \frac{\sigma U^2}{2\Theta_0} \left(\frac{\sigma V^2}{\sigma U^2} - R \frac{\partial}{\partial R} \ln(R \cdot \nu \cdot \sigma U^2) \right), \quad (29)$$

where Θ_0 is the velocity of disk rotation at distance R from the rotation axis; Θ_c , the circular velocity related to the Galactic potential by the following formula

$$\Theta_c^2 = -R \frac{\partial \Phi(R, z)}{\partial R};$$

σU^2 and σV^2 , as above, are the radial and tangential dispersions of peculiar velocities, respectively, and ν is the disk volume density. Like in the above computations we further assume that vertical velocity dispersion is constant and that the variation of the disk thickness can be neglected. In this case the volume mass density is proportional to surface density, $\nu(R) \sim \Sigma(R) \sim \exp(-R/H_D)$. Furthermore, when computing the derivative

$$\frac{\partial}{\partial R} \ln(R \cdot \nu \cdot \sigma U^2),$$

we take into account the fact that variation of radial velocity dispersion σU^2 with Galactocentric distance is related to the variation of epicyclic frequency

$$\kappa^2 = 4\omega(\omega + \frac{R\omega'}{2}),$$

and surface density $\Sigma(R)$ of the disk by Toomre-like formula (2).

Dehnen and Binney (1998) and Schonrich et al. (2010) showed that asymmetric drift law in the local neighborhood of the Galactic disk can be expressed as

$$\Theta_c - \Theta_0 \approx \frac{\sigma U^2}{80 \text{ km/s}} \equiv \zeta \cdot \sigma U^2,$$

where

$$\zeta \approx \frac{1}{2\Theta_0} \left(\frac{\sigma V^2}{\sigma U^2} - R \frac{\partial}{\partial R} \ln(R \cdot \nu \cdot \sigma U^2) \right) \approx \frac{1}{80} \frac{s}{\text{km}}.$$

After simple manipulations with above expressions, we obtain

$$H_D \approx \frac{3R}{2\Theta_0 \zeta + 1 - \frac{\sigma V^2}{\sigma U^2} - \frac{5R\omega\omega' + (\omega'^2 + \omega\omega'')R^2}{\omega(2\omega + R\omega')}}. \quad (30)$$

We then substitute our inferred values of the Galactic rotation curve parameters into expression (30) to estimate the radial scale as

$$H_D \approx (2.7 \pm 0.20) \text{ kpc}; \quad (31)$$

the standard error was calculated via Monte-Carlo method taking into account all errors of other parameters that appear in the formula for the disk scale H_D .

This value of the exponential scale of intermediate-age disk agrees well with the Dehnen and Binney (1998) estimate based on simple exponential variation of radial velocity dispersion; with the dynamic estimates obtained by Khoperskov and Tyurina (2003) (~ 3 kpc), McMillan (2011) (3.0 ± 0.22 kpc), Reid et al. (2014) (2.44 ± 0.16 kpc), McGaugh (2016) ($2.0 - 2.9$ kpc), and with the results of an analysis of the space distribution of stars based on SDSS data performed by Juric et al. (2008) (2.6 ± 0.52 kpc). Note, however, that our estimates are appreciably smaller than that obtained by Benjamin et al. (2005) (3.9 ± 0.6 kpc) based on the data about the distribution of stars of the GLIMPSE IR survey, and somewhat greater than the recent model dynamic estimate obtained by Bovy and Rix (2013) (2.15 ± 0.14 kpc), which is based, among other things, on the data about the space distribution of stars.

Our estimates of the exponential scale of maser disk

based on the assumption of a Toomre-like “equation of state” (2),

$$H_D \approx (4.3 \pm 0.8) \text{ kpc}; \quad (32)$$

(see Tables 1 and 2) are appreciably larger than (31). The maser disk seems to be more homogeneous along Galactocentric radius, and Models C1 – C2 provide a better description of the young disk kinematics. It is appropriate to note that estimate (31) involves local properties of the velocity field, whereas (32) uses only global kinematics of maser sample.

4.4 Local surface density of the thin disk

We can now use the assumption that the intermediate-age Galactic disk is marginally stable to estimate the minimum local surface disk density by the Toomre criterion (evidently, taking into account the fact that the average radial velocity dispersion of most of the disk stars is appreciably higher than the velocity dispersion of masers (~ 10 km/s), which represent the youngest population of the Galactic disk):

$$\Sigma(R_0) > \frac{\kappa(R_0) \cdot \sigma U_0}{3.36G} \approx (26 \pm 3) M_\odot \text{pc}^{-2}.$$

The standard error is estimated using Monte-Carlo technique based on our inferred errors of other parameters. The characteristic radial velocity dispersion for the sample of classical Cepheids younger than 150 Myr is (13 – 15) km/s (Zabolotskikh et al. 2002; Bobylev 2016), and it is even higher for older stars. It is therefore safe to assume that the total local surface disk density should be at least twice greater than the above estimate and amount to (50 – 60) $M_\odot \text{pc}^{-2}$.

Local surface density was estimated in many studies. Let us mention only the relatively recent ones. Thus Korchagin et al. (2003) reported a broad interval of local surface density estimates based on the distribution of old red giants: $(10 - 42) \pm 6$ $M_\odot \text{pc}^{-2}$, with the local volume mass density equal to $\sim 0.1 M_\odot \text{pc}^{-3}$. Bienaymé et al. (2006) estimate the local surface density to be (57 – 79) $M_\odot \text{pc}^{-2}$ within the 1.1 kpc-thick layer. Flynn et al. (2006) estimate the local surface density as $\sim 49 M_\odot \text{pc}^{-2}$ as a result of their studies involving modelling of the mass-to-luminosity ratio of our Galaxy $\sim 49 M_\odot \text{pc}^{-2}$. McGaugh (2016) obtained a dynamic estimate of (34 – 61) $M_\odot \text{pc}^{-2}$ for the average surface density at the solar ring based on their modeling of the terminal velocity curve. Finally, Joshi et al. (2016) estimate the local surface mass density as $\sim 40 \pm 12 M_\odot \text{pc}^{-2}$ from their estimate of the scaleheight of open clusters younger than 0.8 Gyr and located within 0.4–2.0 kpc heliocentric distance interval and combined with adopted Oort’s constant estimates of $A = 14.8$ km/s/kpc and $B = 14.8$ km/s/kpc. It can be easily seen that our lower estimate of local surface density agrees well with other determinations.

5 CONCLUSIONS

We analyzed the kinematics of the youngest disk population using the currently most extensive sample of Galactic masers. This is the first time that the method of statistical parallaxes in its most general form ((Murray 1983;

Rastorguev 2002; Dambis 2009)) is used to study the kinematics of the youngest population of the Galactic disk. We applied this method to a sample of 131 maser sources located in star-forming regions. The proposed method most adequately accounts for all errors in the initial observational data (random and systematic distance errors, random errors of line-of-sight velocities and proper motions), as well as systematic (rotation of the disk and perturbations due to the density wave) and random (ellipsoidal distribution of residual space velocities) motions in the sample, and the errors of the model velocity field due to the random and systematic errors of object distances. As a result, the distribution of the difference between the observed and model velocities of each object is described by the matrix of covariances, which includes both the observed quantities and the full set of parameters to be determined. To determine the unknown parameters we used the method of minimization of the likelihood function.

Because of the large radial extent of the sample we had to take into account the variation of the form and size of the ellipsoid of residual velocities with Galactocentric distance. To this end, we considered three cases: **(A)** Toomre-like “equation of state” (2), **(B)** simple exponential decrease of radial velocity dispersion (3) and **(C)** constant radial velocity dispersion. We further assume that the ratio of the two horizontal axes of the ellipsoid of residual velocities obeys the Lindblad relation (1), i.e., is determined by the current local values of angular velocity and epicyclic frequency.

The main results of this study are:

(1) The distance scale of maser sources based on VLBI trigonometric parallaxes practically needs no systematic correction despite rather substantial random errors of maser parallaxes amounting in the average to 5 – 7%.

(2) The maximum-likelihood method yields the following estimates of the main parameters of the Galactic disk: solar Galactocentric distance (8.24 ± 0.12) kpc, mean components of the maser sample relative the Sun, ($U_0 \approx -11.0 \pm 1.3$, $V_0 \approx -19.0 \pm 1.2$, $W_0 \approx -9.0 \pm 1.1$) km/s. The best fit to the data is provided by Model C with constant velocity dispersions, ($\sigma U_0 \approx 9.4 \pm 0.9$, $\sigma W_0 \approx 5.9 \pm 0.8$) km/s.

We determined the rotation curve of the Galactic disk over the Galactocentric distance interval 3 – 15 kpc and found the rotation velocity at the solar distance to be $(235 - 238) \pm 7$ km/s, which agrees well with the results of Reid et al. (2014). The rotation curve remains practically flat from 5 – 6 out to 15 kpc.

(3) We determined the pitch angle (-10.4 ± 0.3)° and the phase of the Sun (125 ± 10)° of the four-armed trailing spiral pattern in terms of the linear density-wave theory ((Lin and Shu 1964; Lin et al. 1969)). These estimates are in excellent agreement with the results of the investigation of the space distribution of classical Cepheids in the Galaxy (Dambis et al. 2015). We calculate the radial and tangential amplitudes of the perturbations due to the spiral pattern ($f_R \approx -6.9 \pm 1.2$, $f_\Theta \approx +2.8 \pm 1.0$) km/s. According to our data, the global spiral pattern with a pattern speed of $\Omega_P \sim 25$ km/s/kpc (Dambis et al. 2015) may exist in the Galactocentric distance interval 6 – 13 kpc with the corotation near 9.5 – 10 kpc.

(4) We used Jeans hydrodynamic equations and detailed data about the kinematics of stars in the local neighborhood (Dehnen and Binney 1998; Schonrich et al. 2010),

i.e., about the “lag” of centroids of flat subsystems relative to the LSR, to independently estimate the exponential scale of intermediate-age disk. The result $H_D \approx (2.7 \pm 0.20)$ kpc agrees well with others estimates made by different methods. Based on these considerations we obtained a lower estimate for the disk surface density, $(26 \pm 3) M_\odot pc^{-2}$, which, on the whole, is consistent with other published estimates of the total local surface density.

ACKNOWLEDGEMENTS

A.T. Bajkova and V.V. Bobylev acknowledge the support from the Presidium of the Russian Academy of Sciences (Program P-41 “Transitional and explosive processes in astrophysics”). A.S. Rastorguev, N.D. Utkin, M.V. Zabolotskikh, and A.K. Dambis acknowledge the support of the analysis of maser kinematics from the Russian Science Foundation (grant no. 14-22-00041) and the support of the acquisition of observational data from the Russian Foundation for Basic Research (grant no. 14-02-00472). A.K. Dambis acknowledges the support from joint grant by the Russian Foundation for Basic Research and Department of Science and Technology of India through project no. RFBR 15-52-45121 and INT/RUS/RFBR/P-219. The authors are very grateful to the anonymous referee for extremely valuable notes and criticism which made this paper more readable and well-grounded.

APPENDIX

Table 5 provides the data for 38 additional maser sources not included in the last list of Reid et al. (2014). The table contains the J2000 equatorial coordinates, trigonometric parallaxes π and their errors σ_π , proper motion components μ_α , μ_δ and their errors σ_α , σ_δ , radial velocities V_{LSR} relative to the LSR and their errors σ_{V_r} . The last column gives the references to individual maser data.

Note: The last two maser sources in the Table 5 were presented in original list of Reid et al. (2014), but here we present improved data adopted from new studies.

References in Table 5:

- 1 - Choi et al. (2014);
- 2 - Imai et al. (2012);
- 3 - Chibueze et al. (2014);
- 4 - Kusuno et al. (2013);
- 5 - Sakai (2014);
- 6 - Xu et al. (2013);
- 7 - Dzib et al. (2010);
- 8 - Honma et al. (2012);
- 9 - Burns et al. (2014);
- 10 - Reid et al. (2011);
- 11 - Miller-Jones et al. (2009);
- 12 - Burns et al. (2014);
- 13 - Dzib et al. (2011);
- 14 - Torres et al. (2012);
- 15 - Torres et al. (2007);
- 16 - Torres et al. (2009);
- 17 - Loinard et al. (2007);
- 18 - Kamezaki et al. (2014);
- 19 - Kim et al. (2008);
- 20 - Reid et al. (2014);
- 21 - Nagayama et al. (2015);
- 22 - Motogi et al. (2015);
- 23 - Krishnan et al. (2015);
- 24 - Nakanishi et al. (2015);
- 25 - Burns et al. (2015);
- 26 - Dzib et al. (2016);
- 27 - Xu et al. (2016);
- 28 - Nakanishi et al. (2015);
- 29 - Burns et al. (2016);
- 30 - Ortiz-Leon et al. (2016);
- 31 - Krishnan et al. (2016).

□

Table 5. Additional list of 40 maser sources.

Name	RA J2000 hh mm ss	Decl J2000 dd mm ss	π	σ_π mas	μ_α mas/y	σ_α	μ_δ mas/y	σ_δ	V_{LSR} km/s	σ_{V_T}	Ref.#
G170.66–00.25 IRAS 05168+3634	05 20 22.07	+36 37 56.6	0.537	0.038	0.23	1.07	-3.14	0.28	-15.5	1.9	1
G108.43+00.89 IRAS 22480+6002	22 49 58.87	+60 17 56.7	0.400	0.025	-2.58	0.33	-1.91	0.17	-50.8	3.5	2
G110.19+02.47 IRAS 22555+6213	22 57 29.81	+62 29 46.9	0.314	0.070	-2.04	0.35	-0.66	0.36	-63.0	6.0	3
G115.06–00.05 PZ Cas	23 44 03.28	+61 47 22.2	0.356	0.026	-3.70	0.20	-2.00	0.30	-36.2	0.7	4
G119.80–06.03 IRAS 00259+5625	00 28 43.51	+56 41 56.9	0.412	0.123	-2.48	0.32	-2.85	0.65	-38.3	3.1	5
G031.56+05.33 EC 95 Serp	18 29 57.89	+01 12 46.1	2.291	0.038	3.599	0.026	-8.336	0.030	9.0	3.0	6, 7, 8, 30
G071.31+00.83 IRAS 20056+3350	20 07 31.25	+33 59 41.5	0.213	0.026	-2.62	0.33	-5.65	0.52	9.0	1.0	9
G071.33+03.07 Cyg X-1	19 58 21.67	+35 12 05.7	0.539	0.033	-3.78	0.06	-6.40	0.12	13.1	5.0	10
G073.12–02.09 V404 Cyg	20 24 03.82	+33 52 01.9	0.418	0.024	-5.04	0.02	-7.64	0.03	16.9	2.2	11
G074.56+00.85 IRAS 20143+3634	20 16 13.36	+36 43 33.9	0.367	0.037	-2.99	0.16	-4.37	0.43	-1.0	1.0	12
G109.87+02.11 Cep A HW9	22 56 18.64	+62 01 47.8	1.208	0.05	-1.03	0.10	-2.62	0.27	-10.0	3.0	13, 27
G158.06–21.42 L 1448 C	03 25 38.88	+30 44 05.2	4.31	0.33	21.90	0.07	-23.10	0.33	4.5	3.0	6
G158.35–20.56 SVS13/NGC 1333	03 29 03.72	+31 16 03.8	4.25	0.32	14.25	1.00	-8.95	1.40	7.5	5.0	6
G168.22–16.34 V773 Tau	04 14 12.92	+28 12 12.3	7.70	0.19	8.30	0.50	-23.60	0.50	7.5	0.5	14
G168.84–15.52 Hubble 4	04 18 47.03	+28 20 07.4	7.53	0.03	4.30	0.05	-28.90	0.30	6.1	1.7	15
G169.37–15.03 HDE 283572	04 21 58.85	+28 18 06.4	7.78	0.04	8.88	0.06	-26.60	0.10	6.0	1.5	15
G175.73–16.24 HP Tau/G2	04 35 54.16	+22 54 13.5	6.20	0.03	13.85	0.03	-15.40	0.20	6.8	1.8	16
G176.23–20.89 T Tau N	04 21 59.43	+19 32 06.4	6.82	0.03	12.35	0.04	-12.80	0.05	7.7	1.2	17
G203.32+02.05 NGC 2264	06 41 09.86	+09 29 14.7	1.356	0.098	-1.00	0.60	-6.00	3.00	7.1	3.0	18
G208.99–19.38 Orion KL	05 35 14.51	-05 22 30.5	2.39	0.030	9.56	0.10	-3.83	0.15	5.0	5.0	19
G353.02+16.98 DoAr21	16 26 03.02	-24 23 36.4	8.20	0.37	-26.47	0.92	-28.23	0.73	3.0	3.0	6
G353.10+16.89 S1	16 26 34.17	-24 23 28.5	8.55	0.50	-3.88	0.69	-31.55	0.50	3.0	3.0	6
G353.94+15.84 IRAS 16293-2422	16 32 22.85	-24 28 36.4	5.6	1.1	-20.60	0.70	-32.40	2.00	4.4	5.0	6
G045.37–00.22 GRS 1915+105	19 15 11.54	+10 56 44.7	0.116	0.024	-3.19	0.03	-6.24	0.05	30.4	1.0	20
G048.99–00.30 AGAL048.99-0.29	19 22 26.13	+14 16 39.1	0.178	0.017	-2.16	0.09	-5.87	0.17	66.3	0.3	21
G353.27+00.64 NGC 6357	17 26 01.59	-34 15 14.9	0.59	0.06	0.47	0.07	0.99	1.04	-5.0	5.0	22
G339.88–01.26	16 52 04.67	-46 08 34.4	0.48	0.08	-1.60	0.10	-1.90	0.10	-38.8	5.0	23
G095.30–00.94 IRAS 21379+5106	21 39 40.80	+51 20 35.0	0.262	0.031	-2.74	0.08	-2.87	0.18	-42.3	0.2	24, 28
G173.72–02.70 S235AB-MIR	05 40 53.38	+35 41 48.4	0.63	0.03	0.79	0.12	-2.41	0.14	-17.91	3.1	25
G213.88–11.84 Mon2	06 10 50.59	-06 11 50.4	1.12	0.05	-5.32	0.07	0.50	0.10	11.0	1.0	26
G213.70–12.60 Mon R2	06 07 47.86	-06 22 56.5	1.166	0.021	-1.25	0.09	2.44	0.28	10.0	3.0	27
G054.10–00.08	19 31 48.80	+18 42 57.1	0.231	0.031	-3.13	0.48	-5.57	0.48	40.0	3.0	27
G058.77+00.64	19 38 49.13	+23 08 40.2	0.299	0.040	-2.70	0.10	-6.10	0.21	33.0	3.0	27
G059.47–00.18	19 43 28.35	+23 20 42.5	0.535	0.024	-1.83	1.12	-6.60	1.12	26.0	3.0	27
G059.83+00.67	19 40 59.29	+24 04 44.2	0.253	0.024	-2.92	0.07	-6.03	0.05	34.0	3.0	27
G071.52–00.38	20 12 57.89	+33 30 27.1	0.277	0.013	-2.48	0.04	-4.97	0.07	11.0	3.0	27
G192.60–00.04 S255IR-SMA1	06 12 54.02	+17 59 23.3	0.563	0.036	-0.13	0.20	-0.06	0.27	6.0	5.0	29
G108.18+05.51 L 1206	22 28 51.41	+64 13 41.2	1.101	0.033	0.16	0.09	-2.17	0.35	-11	3.0	27
G305.200+0.019	13 11 16.93	-62 45 55.1	0.25	0.06	-6.69	0.03	-0.60	0.14	-33.1	3.0	31
G305.202+0.208	13 11 10.49	-62 34 38.8	0.25	0.05	-7.14	0.17	-0.44	0.21	-44.0	3.0	31

REFERENCES

- Baba J., Asaki Y., Makino J., Miyoshi M., Saiton R., Wada K., 2009, *ApJ*, 706, 471
- Bajkova A.T., Bobylev V.V., 2012, *AstL* 38, 549
- Bajkova A.T., Bobylev V.V., 2013, *AN* 334, 851
- Benjamin R.A., Churchwell E., Babler B.E. et al., 2005, *Astrophys. J.*, 630, L149-L152
- Battinelli P., Demers S., Rossi C., Gigoyan K.S., 2013, *ApJ* 765, 68
- Bhattacharjee P., Chaudhury S., Kundu S., 2014, *ApJ* 785, id.63
- Bienaymé O., Soubiran C., Mishenina T.V., Kovtyukh V.V., Siebert A., 2006 *A&A* 446, 933
- Bobylev V.V., 2004, *AstL* 30, 159
- Bobylev V.V., 2016, arXiv:1611.01766
- Bobylev V.V., Goncharov G.A., Bajkova A.T., 2006, *ARep* 50, 733
- Bobylev V.V., Bajkova A.T., Lebedeva S.V., 2007, *AstL* 33, 720
- Bobylev V.V., Bajkova A.T., Stepanishchev A.S., 2008, *AstL* 34, 515
- Bobylev V.V., Stepanishchev A.S., Bajkova A.T., Gontcharov G.A., 2009, *AstL* 35, 836
- Bobylev V.V., Bajkova A.T., 2010, *MNRAS* 408, 1788
- Bobylev V.V., Bajkova A.T., 2013a, *AstL* 39, 532
- Bobylev V.V., Bajkova A.T., 2013b, *AstL* 39, 759
- Bobylev V.V., Bajkova A.T., 2013c, *AstL* 39, 809
- Bobylev V.V., Bajkova A.T., 2014a, *MNRAS* 437, 1549
- Bobylev V.V., Bajkova A.T., 2014b, *AstL* 40, 389
- Bobylev V.V., Bajkova A.T., 2014c, *AstL* 40, 773
- Bobylev V.V., Bajkova A.T., 2015, *MNRAS* 447, L50
- Bovy J., Hogg D.W., Rix H.-W., 2009, *ApJ* 704, 1704
- Bovy J., Prieto C.A., Beers T.C., Bizyaev D. et al., 2012, *ApJ* 759, id.131
- Bovy J., Rix H.-W., 2013, *ApJ* 779, id.115

- Brand J., Blitz L., 1993, *A&A* 275, 67
- Brown A.G.A., Vallenari A., Prusti T. et al., 2016, arXiv: 1609.04172
- Brunthaler A., Reid M.J., Menten K.M., et al., 2011, *AN* 332, 461
- Burns R.A., Nagayama T., Handa T., Omodaka T. et al., 2014, *ApJ* 797, 39
- Burns R.A., Yamaguchi Y., Handa T., et al., 2014, *PASJ* 66, 102
- Burns R.A., Imai H., Handa T., et al., 2015, *MNRAS* 453, 3163
- Burns R.A., Handa T., Nagayama T., et al., 2016, *MNRAS* 460, 283
- Burton W.B., Gordon M.A., 1978, *A&A* 63, 7
- Chemin L., Renaud F., Soubiran C., 2015, *A&A* 578, id.A14
- Chibueze J.O., Sakanoue H., Nagayama T., Omodaka T. et al., 2014, *PASJ* 66, 104
- Choi Y.K., K. Hachisuka K., Reid M.J., Xu Y., Brunthaler A., Menten K.M., and Dame T.M., 2014, *ApJ* 790, 99
- Dambis A.K., Melnik A.M., Rastorguev A.S., 1995, *AstL* 21, 291
- Dambis A.K., Melnik A.M., Rastorguev A.S., 2001a, *AstL* 27, 58
- Dambis A.K., Glushkova E.V., Melnik A.M., Rastorguev A.S., 2001b, *A&AT* 20, 161
- Dambis A.K., 2009, *MNRAS* 396, 553
- Dambis A.K., Berdnikov L.N., Efremov Yu.N., Kniazev A.Yu. et al. 2015, *AstL* 41, 489
- Dehnen W., Binney J.J., 1998, *MNRAS* 298, 387
- Demers S., Battinelli P., 2007, *A&A* 473, 143
- Dzib S., Loinard L., Rodriguez L.F., et al., 2011, *ApJ* 733, 71
- Dzib S., Loinard L., Mioduszewski A.J., Boden A.F. et al., 2010, *ApJ* 718, 610
- Dzib S.A., Ortiz-Leon G.N., Loinard L., et al. 2016, *ApJ* 826, 201
- Eisenstein D., Weinberg D.H., Agol E., Aihara H., 2011, *AJ* 142, 72
- Fich M., Blitz L., Stark A.A., 1989, *ApJ* 342, 272
- Flynn C., Holmberg J., Portinary L., Fuchs B., Jahreiß H., 2006, *MNRAS* 372, 1149
- Glushkova E.V., Dambis A.K., Melnik A.M., Rastorguev A.S., 1998, *A&A* 329, 514
- Glushkova E.V., Dambis A.K., Rastorguev A.S., 1999, *A&AT* 18, 349
- Hachisuka K., Choi Y.K., Reid M.J., Brunthaler A., Menten K.M., Sanna A., and Dame T.M., 2015, *ApJ* 800, id 2
- Hirota T., Bushimata T., Choi Y.K., et al., 2007, *PASJ* 59, 897
- Honma M., Nagayama T., Ando K., et al., 2012, *PASJ* 64, 136
- Hawley S.L., Jeffreys W.H., Barnes T.G. III, Wan Lai, 1986, *AJ*, 302, 626-631
- Imai H., Sakai N., Nakanishi H., et al., 2012, *PASJ* 64, 142
- Joshi Y.C., Dambis A. K., Pandey A. K., Joshi S, 2016, *A&A* 593, 116
- Juric M., Ivezić Z., Brooks A. et al., 2008, *Astrophys. J.*, 673, 864-914
- Kamezaki T., Imura K., Omodaka T., Handa T. et al., 2014, *APjSS* 211, 18
- Karimova D.K., Pavlovskaya E.D., 1981, *Sov. Astron. Lett.* 7, 111
- Kerr F.J., 1964, "The Galaxy and the Magellanic Clouds", in: *IAU Sympos. No. 20*, 81
- Kerr F.J., 1969, *ARA&A* 7, 39
- Kim M.K., Hirota T., Honma M., et al., 2008, *PASJ* 60, 991
- Khoperskov A.V., Zasov A.V., Tyurina N.V., 2003, *ARep* 47, 357
- Khoperskov A.V., Tyurina N.V., 2003, *ARep* 47, 443
- Korchagin V.I., Girard T.M., Borkova T.V., Dinescu D.I., van Altena W.F., 2003, *AJ* 126, 2896
- Krishnan V., Ellingsen S.P., Reid M.J., Brunthaler A. et al., 2015, *ApJ* 805, 129
- Krishnan V., Ellingsen S.P., Reid M.J., Bignall H.E. et al., 2016, arXiv:1611.00930
- Kusuno K., Asaki Y., Imai H., and Oyama T., 2013, *ApJ* 774, 107
- Levine E.S., Heiles C., Blitz L., 2008, *ApJ* 679, 1288
- Lin C.C., Shu F.H., 1964, *ApJ* 140, 646
- Lin C.C., Yuan C., Shu F.H., 1969, *ApJ* 155, 721
- Loinard L., Torres R.M., Mioduszewski A.J., et al., 2007, *ApJ* 671, 546
- Luri X., Gomez A.E., Torra J., Figueras F., Mennessier M.O., 1998, *A&A* 335, L81
- Lutz T.E., Kelker D.H., 1973, *PASP*, 85, 573
- McGaugh, S.S., 2016, *ApJ*, 816, 42
- McMillan P.J., Binney J.J., 2010, *MNRAS*, 402, 934
- McMillan P.J., 2011, *MNRAS*, 414, 2446-2457
- Melnik A.M., Dambis A.K., Rastorguev A.S., 1999, *AstL* 25, 518
- Melnik A.M., Dambis A.K., Rastorguev A.S., 2001a, *A&AT* 20, 107
- Melnik A.M., Dambis A.K., Rastorguev A.S., 2001b, *AstL* 27, 521
- Melnik A.M., Dambis A.K., 2009, *MNRAS* 400, 518
- Miller-Jones J.C.A., Jonker P.G., Dhawan V., Brisken W. et al., 2009, *ApJ* 706, 230
- Motogi K., Sorai K., Honma M., Hirota T. et al., 2015, arXiv:1502.00376
- Murray C.A., 1983, *Vectorial astrometry*, Bristol: Adam Hilger
- Nagayama T., Kobayashi H., Omodaka T., Murata Y. et al., 2015, *PASJ* 67, 65
- Nakanishi H., Sakai N., Kurayama T., Matsuo M. et al., 2015, *PASJ* 67, 68
- Ortiz-Leon G.-N., Dzib S.A., Kounkel M.A., et al., 2016, arXiv:1610.03128
- Press W.H., Teukolsky S.A., Vetterling W.T., Flannery B.P., 2007, *Numerical Recipes*, 3rd edition, Cambridge University Press, 1256 pp.
- Rastorguev A.S., Glushkova E.V., Dambis A.K., Zabolotskikh M.V., 1999, *AstL* 25, 595
- Rastorguev A.S., Glushkova E.V., Zabolotskikh M.V., Baumgardt H. 2001, *A&AT* 20, 103
- Rastorguev A.S. Using maximum-likelihood method to study the kinematics of galactic populations. <http://lnfm1.sai.msu.ru/~rastor/Study/MaxLikelihood.pdf>, Moscow: Moscow University (electronic tutorial)
- Reid M.J., Moran J.M., 1981, *ARAA* 19, 231
- Reid M.J., Menten K.M., Zheng X.W., et al., 2009, *ApJ* 700, 137

- Reid M.J., McClintock J.E., Narayan R., Gou L. et al., 2011, ApJ742, 83
- Reid M.J., Menten K.M., Zheng X.W., et al., 2014, ApJ 783, 130
- Reid M.J., McClintock J.E., Steiner J.F., Steegh D. et al., 2014, ApJ 796, 2
- Rygl K.L.J., Brunthaler A., Reid M.J., et al., 2010, A&A 511, A2
- Saburova A.S., Zasov A.V., 2014, AN 334, 785
- Sakai N., Sato M., Motogi K., Nagayama T. et al., 2014, PASJ 66,3
- Sanna A., Reid M.J., Menten K.M., Dame T.M., Zhang B., Sato M., Brunthaler A., Moscadelli L., and Immer K., 2014, ApJ 781, 108
- Sato M., Wu Y.W., Immer K., Zhang B., Sanna A., Reid M.J., Dame T.M., A. Brunthaler A., and Menten K.M), 2014, ApJ 793, 72
- Schonrich R., Binney J., Dehnen WW. 2010, MNRAS 403, 1829
- Sofue Y., Honma M., Omodaka T., 2009, PASJ 61, 227
- Sofue Y., 2012, PASJ 64, 75
- Stepanishchev A.S., Bobylev V.V., 2011, AstL 37, 254
- Toomre A., 1964, ApJ, 139, 1217
- Torres R.M., Loinard L., Mioduszewski A.J., et al., 2007, ApJ 671, 1813
- Torres R.M., Loinard L., Mioduszewski A.J., et al., 2009, ApJ 698, 242
- Torres R.M., Loinard L., Mioduszewski A.J., et al., 2012, ApJ 747, 18
- Wilson T.D., Barnes Th.G. III, Hawley S.L., Jefferys W.H., 1991, ApJ 378, 708
- Vallée J.P., 2013, IJAA 3, 20
- Vallée J.P., 2014, AJ 148, art. id.5
- Vallée J.P., 2015, MNRAS 450, 4277
- Wu Y.W., Sato M., Reid M.J., Moscadelli L., Zhang B., Xu Y., Brunthaler A., Menten K.M., Dame T.M., and Zheng X.W., 2014, A&A 566, 17
- Xu Y., Li J.J., Reid M.J., et al., 2013, ApJ 769, 15
- Xu Y., Reid M., Dame T., et al., 2016, arXiv:1610.00242
- Zabolotskikh M.V., Rastorguev A.S., Dambis A.K., 2002, AstL 28, 454